

Local elastic properties of carbon nanotubes in the presence of Stone-Wales defects

N. Chandra, S. Namila, and C. Shet

Department of Mechanical Engineering, FAMU-FSU College of Engineering, Florida State University, Tallahassee, Florida 32312, USA

(Received 25 April 2003; revised manuscript received 29 August 2003; published 2 March 2004)

Carbon nanotubes are being contemplated as reinforcements for the next generation of composite materials. Stress and strain measures at an atomic scale are required to study the effect of inhomogeneities in nanotube based structures. In this work, we have adapted three different stress measures at atomic scales and introduced strain measures as energetically conjugate quantities. These measures are validated for defect free nanotubes and are then used to study the mechanics of 5-7-7-5 topological defects in various single wall nanotubes. It is observed that there is a decrease in the load carrying capacity in the defected region, and this decrease can be attributed to the changes in the kinetics and kinematics in the vicinity of the defects.

DOI: 10.1103/PhysRevB.69.094101

PACS number(s): 62.25.+g

I. INTRODUCTION

The exceptional mechanical properties of carbon nanotubes (CNTs) and their potential use in structural components and devices have stimulated great interest and extensive research, ever since their discovery by Iijima¹ in 1991. The stiffness and strength of CNTs are in the range of TPa and GPa, respectively, while the nearest competing materials exhibit these properties in the range of GPa and MPa, respectively. Also the fact that CNTs are extremely lightweight compared to other materials makes them potential candidates as reinforcing fibers in superstrong composites. Before they can be applied in real nanocomposites, the strength and stiffness of CNTs as stand alone units and their ability to transfer loads between a matrix and the nanotubular fibers through nanoscale interfaces needs to be clearly understood. At the heart of the problem is the very definition of strength and stiffness at these scales. Strength and stiffness are defined based on stresses and strains at the macroscopic continuum level and these definitions are ambiguous at the nanoscopic level. This issue is neither philosophical nor pedagogical but one of practical relevance, as will be illustrated in this paper. Widely reported computational and experimental results of CNT strength and stiffness are based on averaged quantities computed or measured at the length scale of a nanotube which is many orders greater than the local atomic dimensions. Though these averaged quantities may lead to acceptable properties for a few idealized configurations, local measures are required to unequivocally determine certain extremum behaviors such as inelasticity, damage, fracture, and failure. Such is the case when we need to study the origin and effect of deviations from the regular hexagonal arrangement of carbon in a graphene sheet or in carbon nanotubes. Local mechanical behavior, for example in a 5-7-7-5 Stone-Wales defect, is entirely different from that of a region away from the defect, all within the same nanotube subjected to a far field force. The relation between the average and local behaviors is a well-known problem in the macro world but is manifested with even more vigor in the CNT based nanoworld, and is the subject of the present paper. Though we have focused on single walled CNTs in this work, the methodology developed here is equally applicable to multi-walled CNTs. Since we mainly deal with single wall carbon

nanotubes in this work, the term CNT refers to a single wall carbon nanotube unless indicated otherwise.

Experimental observations have revealed that topological defects such as the 5-7-7-5 Stone-Wales defect are commonly present in nanotubes.² These local defects can alter not only the inelastic properties but also the elastic properties, e.g., the Young's modulus and Poisson's ratio. Consequently, these defects may alter the longitudinal, lateral stiffnesses, and flexural rigidity in response to tension, torsion, and bending, respectively. It should be noted that analogous point or line defects (vacancies, substitutional atoms, and dislocations) in bulk crystalline materials tend to influence only the inelastic properties because these types of defects, though quite large in number, are still extremely small volumetrically. Because of the unique planar hexagonal meshlike structure of the carbon nanotubes, topological defects can alter the deformation response and hence the elastic properties. In addition, these can also be potential sites where an irreversible mechanical response is initiated.³ While these assertions are true even for planar graphene sheets, when rolled as carbon nanotubes these defects locally alter the curvature of the tubes causing further nonlinear effects. Consequently, they respond differently not only when the diameter varies, albeit to a lesser extent, compared to the chirality where the rolling orientation directly affects the geometry near the defects.

Studies have shown that defects in CNTs may not only affect the mechanical properties but the electronic, magnetic, and hybridization characteristics, and hence needed to be understood thoroughly.⁴⁻⁶ Also the transition in the Y junction contemplated in CNT based molecular electronics is achieved through the incorporation of many 5-7-7-5 defects either by design or otherwise.⁷ Similarly, a transition of nanotubes from one diameter to another can be achieved by locating a few of these defects strategically in the transition region. In addition, when nanotubes are used as fibers in nanocomposites interfacial bonding may preferably occur in these defects regions based on energy considerations. Thus when studying load transfer issues in CNTs, understanding the mechanics of these zones is critical. Another area of potential application of CNTs is in the effective storage of hydrogen for possible use in fuel cells. Here again the propensity for hydrogen penetrating a defected region and entering the tube is higher than regular regions.

In this paper, we introduce definitions of atomic stress and atomic strain quantities as applicable to carbon nanotubes. Though these stress measures have already been used to compute stresses in general three-dimensional crystalline materials, their application to carbon nanotubes entails a certain re-evaluation of what constitutes the proper volume in a planar configuration. We have formulated a methodology to evaluate the kinematic measure of atomic strain specifically for carbon nanotubes. Strain at the atomic level is still defined as the spatial gradient of the displacement field; the displacement field is expressed in terms of atomic displacements and interpolation functions. These measures are applied to CNTs with and without 5-7-7-5 Stone-Wales defects. Local stress-strain responses in the defected and perfect regions are then examined. It is observed that the defect produces stress and strain concentration effects in the vicinity of the defect due to changes in the geometric configuration and concomitant force fields. The *local stiffness* substantially decreases in the defected region and the mechanics of why this happens is examined in terms of both the kinematics and kinetics.

II. ATOMIC LEVEL STRESS MEASURES

Stress is a measure defined to quantify the internal resistance of a material to counter external disturbances. These external disturbances can be either mechanical, thermal, electrical, magnetic, or gravitational in nature. While mechanical loads appear as forces and moments at the surfaces of the body, other loads are distributed throughout the volume as body forces. Stress in a simplified sense can be construed as force over an infinitesimal area as the area tends to zero in the limiting process. It is implied in this definition that force acting over the infinitesimal area is uniform, leading to a unique state of stress. Without loss of generality this concept of uniform force over an infinitesimal volume can be extended to the three-dimensional state of stress with forces acting on the surfaces of the cube.

When we define stress at a point, in the sense of continuum mechanics we implicitly assume that a homogenous state of stress exists within the appropriately chosen infinitesimal volume surrounding that point. As we apply this concept to *discrete lattice mechanics*, we need to identify a volume around a given point over which the stress becomes homogeneous. Such a selection of appropriate volume clearly depends on the degree of stress heterogeneity existing at the material in question. It should be noted that the heterogeneity in the stress state can be caused either due to the heterogeneity in the material (e.g., defects such as inclusions) or due to inhomogeneous loading conditions (e.g., bending). If stress in a selected volume has a very sharp spatial gradient, then we are required to choose smaller and smaller volumes to evaluate the stress quantity with a clear objective of choosing the largest possible volume to satisfy the condition of homogeneity within that volume.

In this context there have been various formulations of stress in molecular dynamics such as virial stress,⁸ BDT stress,⁹ Lutsko stress,^{10,11} and mechanical stress by Cheung and Yip.¹² We invoke these various definitions of

stress measures with different volumes of interrogation and apply them to carbon nanotubes in a molecular dynamics formulation based on the Brenner potential.¹³ The most commonly used stress measure at the atomic scale is the virial stress⁸ (Σ_{ij}). For a pair potential V this can be expressed as

$$\Sigma_{ij} = \frac{1}{\Omega^{\text{Tot}}} \sum_{\alpha=1,n} \left(\frac{1}{2} m^\alpha v_i^\alpha v_j^\alpha + \sum_{\beta=1,n} \frac{r_{\alpha\beta}^i r_{\alpha\beta}^j}{|r_{\alpha\beta}|} \frac{dV}{dr_{\alpha\beta}} \right). \quad (1)$$

Here i and j denote the indices in Cartesian coordinate systems 1, 2, and 3, while α and β are the atomic indices. The summation is over all the atoms occupying total volume Ω^{Tot} . m^α and v^α denote the mass and velocity of atom α . $r_{\alpha\beta}$ is the distance between atoms α and β . The term $dV/dr_{\alpha\beta}$ is the scalar of force exerted on atom α by atom β . Without loss of generality this expression can be rewritten for potentials dependent on bond angles such as bond order potentials as

$$\Sigma_{ij} = \frac{1}{\Omega^{\text{Tot}}} \sum_{\alpha=1,n} \left(\frac{1}{2} m^\alpha v_i^\alpha v_j^\alpha + \sum_{\beta=1,n} r_{\alpha\beta}^j f_{\alpha\beta}^i \right), \quad (2)$$

where $f_{\alpha\beta}^i$ is the force on atom α due to atom β resolved in the i th direction. We have used this form to calculate virial stress. A similar form for atomic stress has been used for Si modeled with the Tersoff potential by Yu and Madhukar.¹⁴ Based on the preceding discussion regarding volume it may be noted that this stress formulation is strictly valid only when a homogenous stress state exists in the entire volume of the simulation box. For example, this measure would be valid for uniformly loaded nanotubes without defects.

The above definition of bulk stress has been extended to one atomic volume by Basinski, Deusberry, and Taylor⁹ to define atomic stress (also called BDT stress). This is based on the assumption that a bulk stress measure would be valid for a small volume Ω^α around an atom α . This definition of atomic stress (σ_{ij}^α) for atom α can be expressed as

$$\sigma_{ij}^\alpha = \frac{1}{\Omega^\alpha} \left(\frac{1}{2} m^\alpha v_i^\alpha v_j^\alpha + \sum_{\beta=1,n} r_{\alpha\beta}^j f_{\alpha\beta}^i \right). \quad (3)$$

Theoretically, the above definitions are valid only for homogenous systems, though BDT stress gives a fair indication of the nature of stresses in systems with defects and has been used to study point defects and grain boundaries in a number of metallic systems.^{9,15,16} The total volume and volume of a single atom are required for the calculation of virial and BDT stresses. Further, to ensure consistency,

$$\Sigma_{ij} = \frac{1}{\Omega^{\text{Tot}}} \sum_{\alpha} \sigma_{ij}^\alpha \Omega^\alpha. \quad (4)$$

The total volume has been used extensively in the computation of an elastic modulus based on an energy approach (see the references in Table I). We have used the most commonly used volume $\Omega^{\text{Tot}} = \pi d t l$ where d is the diameter, l is the length, and $t = 3.4 \text{ \AA}$ is the interplanar spacing in graphite. The atomic volume has been computed based on the interatomic distance (1.42 \AA in undeformed tubes) and the interplanar spacing (3.4 \AA).

TABLE I. Values of Young's Modulus computed for CNT by different methods in the literature.

Author & Year	Method	Young's Modulus (TPa)	Other Material Parameters	Comments
Hernandez, Goze Bernier, Rubio (1998)	Total-energy, non-orthogonal tight binding. Axial tension	1.22-1.26	Poisson's ratio: 0.18	wall thickness=0.34 nm $Y = V_o^{-1}(\partial^2 E / \partial \epsilon^2)$
Timur Halicioglu (1998)	Molecular dynamics (Brenner's Pot) Axial tension	0.50	Poisson's ratio: 0.18	wall thickness=0.34 nm $Y = (\partial \sigma / \partial \epsilon)_{\epsilon=0}$
Dong Qian, Wing kam Liu and Rodney S. Ruoff (2001)	Analytical method on graphene sheet	0.989	Poisson's ratio: 0.367	wall thickness=0.34 nm $C_{ijkl} = (\partial^2 W / \partial F_{ji} \partial F_{lk})$
Y. Xia, M. Zhao, Y. Ma, M. Ying, X. Liu, P. Liu, and L. Mei (2002)	Molecular dynamics and <i>ab initio</i> Internal pressure	$C(5.5)$ $2.55(\epsilon_{zz} < 0.003)$ $0.85(\epsilon_{zz} < 0.04)$ $1.14(\epsilon_{rr} < 0.003)$ $0.52-0.26-$ $(0.003 < \epsilon_{rr} < 0.04)$	Poisson's ratio used in calculation 0.17	Independent of wall thickness, Y increases with 5-7-7-5 defect
G. Zhou, W. Duan, B. Gu (2000)	First principles cluster method (LDA) Axial tension	0.764	Poisson's ratio: 0.32	Tensile strength=6.249 GPa.
J. P. Lu (1997)	Empirical force constant model	0.971-0.975	Poisson's ratio: 0.277-0.280	wall thickness=0.34 nm
J. M. Molina, S. S. Savinsky, and N. V. Khokhriakov (1995)	Tight binding	1.4	----	wall thickness=0.34 nm
A. Krishnan, E. Dujardin, T. W. Ebbesen, P. N. Yianilos, and M. M. J. Treacy (1998)	Experimental: free standing room temperature vibrations	1.25	-----	Weighted average value
B. I. Yakobson, C. J. Brabec, and J. Bernholc, (2001)	Many body potential and continuum shell model	5.5	Poisson's ratio: 0.19	wall thickness=0.066 nm
B. G. Demczyk, Y. M. Wang, J. Cumings, M. Hetman, W Han, A. Zettl, R. O. Ritchie (2002)	Experimental pull and bend test	0.91	Tensile strength =0.15 TPa	wall thickness=0.334 nm with continuum correction Young's modulus=0.8 TPa
M. F. Yu, B. S. Files, S. Arepalli, R. S. Ruoff (2002)	Experimental Tension test	0.32-1.47	Failure strength: 13-52 GPa	wall thickness=0.34 nm
Z. C. Tu and Z. C. O. Yang (2002)	LDA	4.7	Poisson's ratio: 0.34	wall thickness=0.075 nm
G. V. Lier, C. V. Alsenoy, V. V. Doren, P. Geerlings (2000)	<i>Ab initio</i>	0.72-1.120	Poisson's ratio: 0.026-0.125	wall thickness=0.34 nm
M. M. J. Treacy, T. W. Ebbesen, J. M. Gibbson (1996)	Experimental (TEM)	1.81	-----	First measurement of Y
J. P. Salveta, G. A. D. Briggs, J. M. Bonard, R. R. Bacsa, A. J. Kulik, T. Stockli, N. A. Burnham, and L. Forro (1999)	Experimental (Atomic Force Microscope)	1.0	Shear modulus =1 GPa.	wall thickness=0.34 nm
N. Yao, V. Lordi (1998)	Molecular Dynamics (Thermal vibrational frequencies)	1.0	----	wall thickness=0.34 nm
C. F. Cornwell and L. T. Wille (1997)	Molecular Dynamics (axial Compression)	0.2-2.0	-----	Y varies with radius

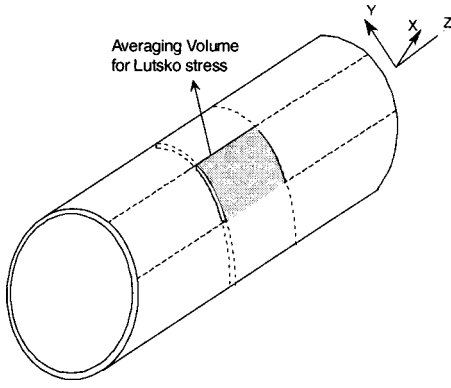


FIG. 1. Averaging volume used for the Lutsko stress in the simulations.

Other definitions of stress have been advanced by Lutsko¹⁰ and Cheung and Yip¹² to study inhomogeneous systems. According to Cheung and Yip's definition, mechanical stress is calculated as the sum of the time rate of the change of the momentum flux and forces divided by area across the particular surface of interest. The concept of local stress advanced by Lutsko and extended by Cormier *et al.*¹¹ is based on the local stress tensor of statistical mechanics. Further, this definition has been shown to conserve linear momentum. The Lutsko stress (σ_{ij}^L) can be expressed as

$$\sigma_{ij}^L = \frac{1}{\Omega^{\text{Avg}}} \sum_{\alpha=1,n} \left(\frac{1}{2} m^\alpha v_i^\alpha v_j^\alpha + \sum_{\beta=1,n} r_{\alpha\beta}^j f_{\alpha\beta}^i \right). \quad (5)$$

Here $l_{\alpha\beta}$ denotes the fraction of the length of α — β bond lying inside the averaging volume Ω^{Avg} . Further, this averaging volume can be a small part of the total volume possibly containing defects. Lutsko stress has been used to evaluate the local elastic properties of grain boundaries in metals. Cormier *et al.*¹¹ have recently shown that this measure gives a better match for continuum solution of inclusion problem.

In bulk materials the averaging volume (for the Lutsko stress) is typically considered as a spherical volume, though the derivation of the stress tensor places no such restriction. We have considered an averaging volume shown in Fig. 1 for this calculation.

In summary, Virial stress can be used if the stress state is homogeneous in the entire volume (of simulation cell); Lutsko stress can be computed for a partial volume and the homogeneity restriction is still applicable to that volume. If the stress needs to be computed around a single atom, then BDT stress can be used. Here again homogeneity is assumed in the volume in which stress is computed. In the converse, if inhomogeneity exists then the choice of the stress measure depends on the extent of spatial inhomogeneity. For example, if we need to examine the overall effect of a 5-7-7-5 Stone-Wales defect, we need to use Lutsko stress. If we are further interested in the role of a specific atom in the defected region, then we need to use BDT stress to capture the physics of the problem.

In spite of the fact that these various definitions have been used with regularity in studying metallic systems (both for EAM and pair potentials), and some nonmetallic systems

such as Si and Ge,¹⁴ to the best of our knowledge they have not been used for carbon nanotubes. For carbon nanotubes, Halicioglu¹⁷ has obtained the atomic stress values in carbon nanotubes based on the strain energy consideration using

$$\sigma_{ij} = \frac{1}{\Omega} \frac{\partial E^\alpha}{\partial \varepsilon_{ij}}. \quad (6)$$

Here E^α is the strain energy and ε_{ij} is the corresponding strain component. This measure is used for the entire tube and requires knowledge of conjugate strain. Belytschko *et al.*¹⁸ calculated stress based on applied forces and the cross sectional area of the nanotube. Xia *et al.*¹⁹ calculated stress based on the pressure exerted by hydrogen atoms in the nanotube and the averaged increase in the dimensions of the nanotube.

The prevailing methods of evaluating elastic moduli and the stress-strain behavior of nanotubes implicitly assume that a homogenous state of stress exists, allowing them to use energy to compute the modulus. Further they need to know the value of the strain and to assume that the strain is constant throughout the domain. This would not pose any problems for nanotubes without defects under uniaxial loading. We show in later sections that when the condition of homogeneity is violated, as in a defected system, or in the case of multiaxial state of loading local stress and strain measures would prove to be more useful than global energy based approaches. Now we proceed to develop the kinematic or strain measure for nanotubes at an atomic scale.

III. ATOMIC LEVEL STRAIN AND ENERGY MEASURES

In the description of continuous media, the thermomechanical behavior of materials is usually prescribed by relating the kinetic quantity at a given material point (or particle) to a kinematic quantity through a constitutive equation. For example, in Hooke's law for isotropic materials the kinematic quantity strain ε is related to the kinetic measure stress σ , using the simple relation $\sigma = E\varepsilon$, where E is the Young's modulus. This modulus is usually evaluated in a uniaxial tensile test where the stress state is uniaxial ($\sigma_{11} = \sigma$) but the strain state is multiaxial ($\varepsilon_{11} = \varepsilon; \varepsilon_{22} = \varepsilon_{33} = -\nu\varepsilon$) and the modulus is $E = \sigma_{11}/\varepsilon_{11} = \sigma/\varepsilon$. The strain energy associated with the deformation is given by

$$dW = \sigma d\varepsilon \Rightarrow W = \frac{\sigma^2}{2E} = \frac{E\varepsilon^2}{2}. \quad (7)$$

If Young's modulus is a constant then the stress-strain response is linear and strain energy in Eq. (7) is valid. Such is the case for a linear elastic isotropic material. The above equation illustrates the fact that in order to evaluate Young's modulus in a linear elastic model, only any two of the variables stress, strain, and energy are independent. While evaluating the former two, many workers used energy and strain to obtain these quantities under homogenous conditions. Young's modulus can be evaluated using energy and some strain measure using the equation,

$$E = \frac{2W}{\epsilon^2} \quad \text{or in general terms as} \quad E = \frac{\partial^2 W}{\partial \epsilon^2}. \quad (8)$$

In the above equation selection of any strain measure ϵ yields a corresponding modulus E , though it can be easily noticed that the pairs are not unique. For example, if one were to select a new measure ϵ^* and then evaluate E^* then this new modulus will be quite different, as shown below:

$$\epsilon^* = \alpha \epsilon, \quad \sigma^* = \beta \sigma \Rightarrow E^* = \gamma E \quad \text{where}$$

$$\gamma = \frac{\beta}{\alpha} \quad \text{given that} \quad \alpha \beta = 1. \quad (9)$$

The above equation holds good for any arbitrary value of α and β . It is thus clear that one can get quite different values of Young's modulus based on the selection of strain measure or stress measure. For the more general case of anisotropic elastic materials, if W is assumed to be a function of only a current deformed state and independent of the history of the deformation then the material is hyperelastic with

$$C_{ijkl} = \frac{\partial^2 W}{\partial \epsilon_{ij} \partial \epsilon_{kl}}, \quad (10)$$

where C_{ijkl} are the components of the fourth order elasticity tensor and ϵ_{ij} are the components of the strain tensor. Unfortunately for the above equation to be consistent with the usual elasticity tensor components one needs to identify ϵ_{ij} as the components of the frame invariant Green-Lagrange strain tensor. Thus evaluating stiffness components using Eq. (10) or (8) has several shortcomings.

(1) The magnitude of the Young's modulus even for isotropic cases, depends on the choice of strain measure, as shown in Eq. (9).

(2) In using Eq. (7) the carbon nanotubes exhibit a directional independence in their material orientations. Clearly this is not the case as the mechanical response of a zigzag tube is different from that of an armchair tube. Thus the equation presumes that a material is isotropic which is incorrect.

(3) The equation implicitly assumes that a state of homogeneous deformation occurs throughout the volume of interrogation, which is not always the case.

(4) We need to implicitly assume that a strain energy density function exists for these classes of materials.

(5) We need to assume that the internal strain energy in the material is always equal to the change in potential energy as given by the interatomic potentials. This would not be true for simulations at a finite temperature.

Based on the above argument, the proposed method of evaluating local stresses and strains is a better approach to the problem. Strain is a measure of the deformation suffered by a body, and is typically measured by the relative changes in length and angles of line segments of the deformed configuration compared to the original. The simplest form of strain is the uniaxial strain defined by $\epsilon = (L - L_o)/L_o$, where L is the current length and L_o is the original length. Though this form of strain has been used for nanotubes,^{18,20}

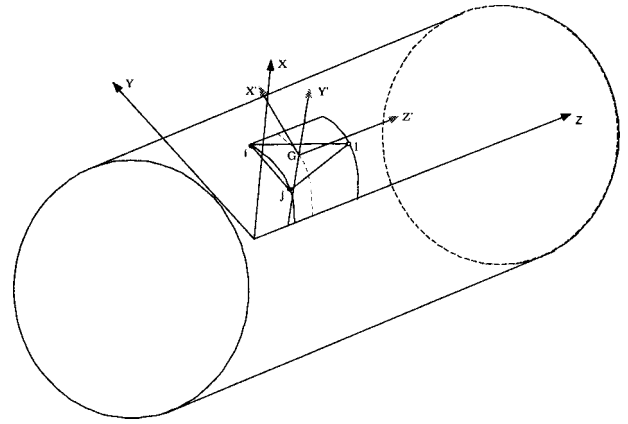


FIG. 2. A typical triangular facet, with the local coordinates (x', y', z') coinciding with the centroid of the triangular element.

it may not be sufficient to represent multiaxial strain state or prove adequate for inhomogeneous distributions.

A more general measure that is applicable to large deformation and finite rotation cases is the deformation gradient tensor F which relates the deformed configuration \mathbf{x} to the undeformed configuration \mathbf{X} given by

$$F = \frac{d\mathbf{x}}{d\mathbf{X}}. \quad (11)$$

The displacement \mathbf{u} of a given atom can be expressed as

$$\mathbf{u} = \mathbf{x} - \mathbf{X}. \quad (12)$$

An infinitesimal strain measure ϵ defined as

$$\epsilon = \frac{\partial \mathbf{u}}{\partial \mathbf{X}} = (\mathbf{F} - \mathbf{I}), \quad (13)$$

is used in this work. For a theoretically consistent formulation one needs to identify a set of frame invariant stress and strain measures that are not only conjugate quantities but are evaluated in the same configuration, either in the undeformed or the deformed state. There are many choices available and the selection criterion is beyond the scope of this paper. However, if we choose to use the deformed configuration as our reference state, then we can use Cauchy stress and Almansi strain as the conjugate quantities. Further, Almansi strain can be approximated to the small strain measure presented above [Eq. (13)], if the strains are not large and if the rigid body rotations during the deformations are limited.

The computational methodology for calculating strains is as follows: a defect free nanotube can be considered as a mesh of hexagons. Each of these hexagons can be treated as containing four triangles. A local coordinate system $(X'Y'Z')$ is constructed for each of these triangles with a centroid as the origin, and the local Z' axis is along the length of tube (see Fig. 2), the local Y' coincides with the radial direction of the centroid of the triangle. The local X' is obtained as cross product of Z' and Y' axes, so that atoms lie on the $X' - Z'$ plane. The in-plane strains $(\epsilon_{z'}, \epsilon_{x'}, \epsilon_{z'x'})$ for this configuration can be evaluated using displacements of atoms i, j , and $l (u_i, v_i, \dots)$ which form the triangle as

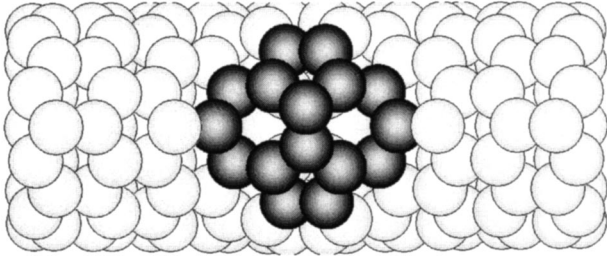


FIG. 3. (9,0) tube containing a 5-7-7-5 defect of type I.

$$\begin{Bmatrix} \varepsilon_{z'} \\ \varepsilon_{y'} \\ \gamma_{z'y'} \end{Bmatrix} = [B] \{u_i \ v_i \ u_j \ v_j \ u_l \ v_l\}^T,$$

where $[B]$ is the matrix of the gradient of the interpolation functions.²¹ Once the strains of the triangular facets are obtained, strains in hexagons are evaluated as the area weighted average of the triangles contained in the hexagons. In the case of tubes with 5-7-7-5 defects the mesh described above contains heptagons and pentagons along with hexagons. These pentagons and heptagons are composed of three and five triangular facets respectively. The strain at each atomic location is evaluated as average of three hexagons (or heptagons/pentagons) that encompass the concerned atom.

IV. RESULTS AND DISCUSSION

In this section we present results obtained from molecular static simulations using conjugate gradient algorithm and Brenner potentials. Periodic boundary conditions were applied to model tubes of infinite length. For simulating CNTs under uniaxial loading, displacements were applied to the atoms in the longitudinal direction. Stress, strain, and energy measures at the local and global levels were computed for all cases. In order to validate the local stress and strain measures, a perfect (9,0) CNT was analyzed. Once validated, these measures are used to study the 5-7-7-5 defect in tubes with different diameters and chiralities.

In zigzag ($n,0$) nanotubes 5-7-7-5 defects can be manifested in two different types, type I and type II, as shown in Figs. 3 and 4. In a type I defect, a horizontal bond of a hexagonal network is rotated by 90° so that when the defect is formed, two of the hexagons are transformed to two heptagons and two pentagons, placed symmetrically about x (or y)- z axes. In the type II defect heptagons and pentagons are asymmetric with x (or y)- z axes.

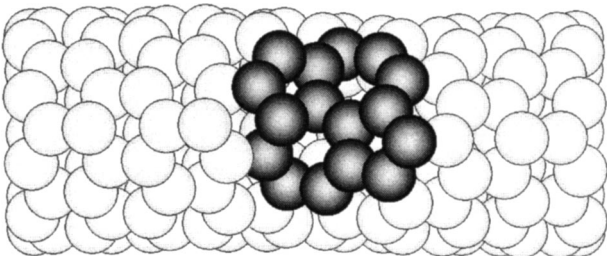


FIG. 4. (9,0) tube containing a 5-7-7-5 defect of type II.

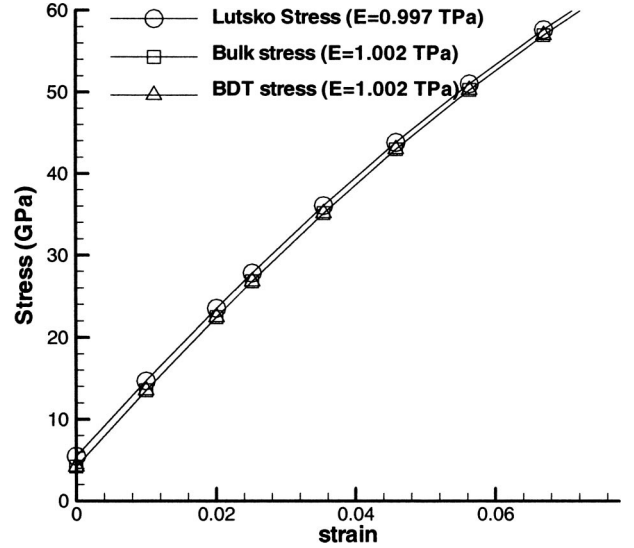


FIG. 5. Stress-strain curve for a (9,0) perfect tube subject to uniaxial tension based on three stress measures.

A. Validation of stress and strain measures

When subjected to a far field, load on a defect free homogenous state of stress and strain exists. Strain calculations based on a triangular facet approach give consistent results for tubes with different chiralities and diameters. Also the three stress measures yield consistent stress values. For a tube with uniform strain, the variation in BDT stress (computed for each atom) from atom to atom is negligible, and the magnitude of BDT stress and virial stress are found to be identical. For homogenous systems by definition, virial and BDT stresses coincide, since the volume Ω^{tot} in Eq. (2) is equal to $n\Omega^\alpha$ in Eq. (3) where n is the number of atoms in the system. When Lutsko stress is computed, a volume slightly larger than twice cutoff radius is used. The additional $l^{\alpha\beta}$ term [see Eq. (4)] leads to a small difference between Lutsko and virial stresses. If we choose a larger volume for the Lutsko stress, the difference reduces and completely vanishes when the interrogating volume is equal to total volume. However, the slope of the stress-strain curve in all the three cases is identical.

It is interesting to note that the strain values in the triangles are not necessarily equal to the applied strain values. Though the magnitude of strain in adjacent triangles is different, the weighted average of strain in any hexagon is the same, and is identical to the applied strain. Consequently, every atom experiences the same state of strain. The variation of the strain state within the hexagon (in different triangular facets) is a consequence of different orientations of interatomic bonds with respect to the applied load axis.

Further, to validate the applicability of the three stress measures and the strain measure, stress-strain curves are plotted for a perfect (9,0) CNT under uniaxial tension. Figure 5 shows the stress-strain curves based on virial, Lutsko, and BDT stresses, measured in the longitudinal (Z) direction, and longitudinal strain ε_z . The Young's modulus is evaluated as the slope of stress-strain curve at zero strain (initial tangent). We obtain a Young's modulus value of 1.002 TPa for a (9,0)

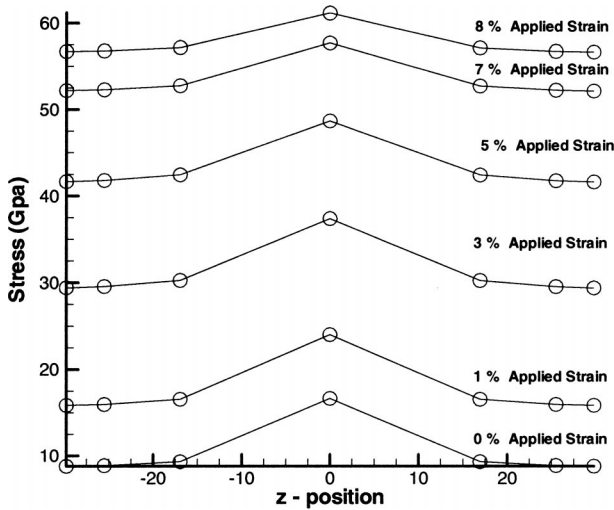


FIG. 6. Variation of Lutsko's stress along the length of a (9,0) SWCNT containing a 5-7-7-5 defect of type I near the center of the tube.

CNT. This compares favorably with values published in the literature as shown in Table I. Though there is a wide variation in the value of the Young's modulus (0.5–5.5 TPa), based on different computational and experimental approaches, the value centers around 1 TPa which compares well with this investigation.^{22–33}

Having validated the stress and strain measures, in Sec. IV B we present the mechanical response of nanotubes with 5-7-7-5 defects. The results are then followed by a discussion of interesting observations in Sec. IV C

B. Deformation of nanotubes with a 5-7-7-5 defect

Figure 6 shows the variation of Lutsko stress σ_{33} along the length of the (9,0) tube. The tube has a symmetric 5-7-7-5 defect placed in the middle of the tube. The nanotube is divided into seven segments along the length, and a strip of atoms in each segment as shown in Fig. 1, is selected for computing average stresses and strains. It can be clearly observed from Fig. 6 that there is a stress amplification in the central segment which contains the defect. We note that even at zero strain level, a stress value of about 15 GPa is observed at the defect, analogous to residual stresses at macro scales. As the strain level increases, the stress concentration factor (defined as the ratio of peak stress to average stress) decreases.

Figure 7 shows the variation of longitudinal strain ϵ_{33} along a length of a CNT for different strain levels. At a 0% external strain, the local strains at all points are equated to zero and form the reference configuration against which further deformation is measured. Though it is possible to use other reference states (for example, a defect-free CNT with a hexagonal network) the present choice is preferred since displacements are identically zero. With this definition of the initial state, the strain is zero, in not only defect free hexagons, but also in pentagons and heptagons.

From Fig. 7, it can be observed that magnitude of the strain increases at the defect and is uniform away from the

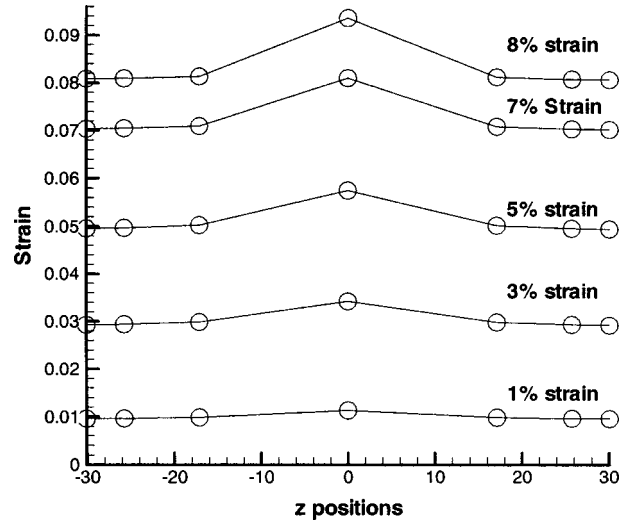


FIG. 7. Variation of strain ϵ_{33} along the length of a (9,0) SWCNT containing a 5-7-7-5 defect of type I near the center of the tube.

defect. The longitudinal strain response is considerably different from that of the stress. The strain concentration (defined as the ratio of local to the global average) increases with increase in externally applied load, while the stress concentration is found to decrease with increasing applied strain. The shear strains are equal to zero in nanotubes without defects but a small amount of shear (about one tenth of applied strain) is present in defected tubes. This effect is found to extend to the areas adjoining defected region.

Since the local values of the stress and strain vary for each of the atoms in the defected region, it is useful to examine the spatial variation of these quantities using a contour plot. Figure 8 shows the stress and strain contour plots near the defected region for various applied strains. Stress contours are based on BDT (atomic) stresses and correspond to the strain states which are also computed at each atom. Both stress and strain contours show concentration effects on the rotated bond that engenders the type I defect. Though not shown here, peak stress occurs at the defect even at zero applied strain and this corresponds to the stress caused due to the presence of defect. Contour plots show that both stress and strain values monotonically increase though there are some differences in their responses.

Use of Lutsko stress enables us to examine the stress-strain response of the defected region per se and compare it with the properties of a defect free CNT. Figure 9 shows Lutsko stress-strain curves for a defect free (9,0) nanotube [plot (a)] and compares it with the Lutsko stress-strain curves of the defected regions. From this plot it can be observed that there is a drop in stiffness at the defect. The stiffness of region with type I defect [plot (b)] is 0.621 TPa and that of type II defect [plot (c)] is 0.627 TPa in contrast to a much higher Young's modulus value of 1.002 TPa for a defect free CNT.

We now proceed to compare the effect of defects on mechanical properties for various diameters. The numerical values of stiffness of defected regions in different CNTs are tabulated in Table II, and Fig. 10 shows the stress-strain

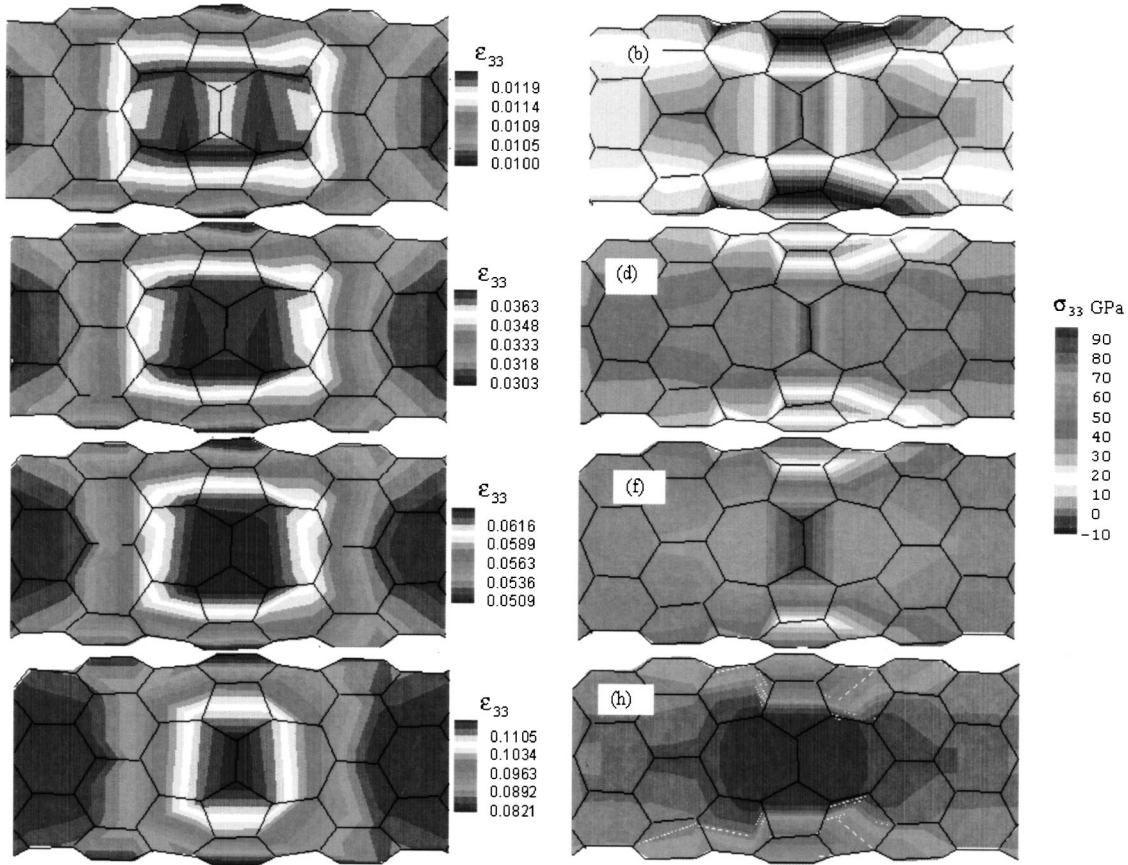


FIG. 8. Contour plots of the longitudinal strain ϵ_{33} strain and stress σ_{33} near the defected region drawn at different applied strain levels. (a) Strain contours at an applied strain of 1%. (b) Stress contours at an applied strain of 1%. (c) Strain contours at an applied strain of 3%. (d) Stress contours at an applied strain of 3%. (e) Strain contours at an applied strain of 5%. (f) Stress contours at an applied strain of 5%. (g) Strain contours at an applied strain of 8%. (h) Stress contours at an applied strain of 8%.

curves. There is only a marginal difference in the local stiffness values for various $(n,0)$ CNTs.

C. Discussion

It is quite noteworthy that even for fully equilibrated defect free CNTs, a nonzero stress of a few GPa is observed at zero strain (see Figs. 9 and 10). This can be construed as residual stresses which are defined as self equilibrating internal stresses even in the absence of external loads (thermal or mechanical). If these nonzero residual stresses are caused by the geometry of formation, then the magnitude of stress should depend on the diameter. Figure 11 shows the variation of zero-strain stresses with an inverse of the radius for various $(n,0)$ type CNTs. It can be seen from Fig. 11 that these stresses decrease monotonically with the radius of CNTs and approach zero for an infinite radius, i.e., a graphene sheet. Since these stresses vanish for a graphene sheet and increase with the curvature, these stresses can be considered formation stresses relative to a graphene sheet and hence formation induced residual stresses. The residual stresses should also correspond to strain energy relative to graphene sheets and are supported by the results of Robertson *et al.*³⁴

Further, in nanotubes with defects at zero strain, there is an additional stress (and hence energy) that corresponds to

the formation of defects (see Fig. 6). Thus in defected regions residual stresses arise both due to the curvature and defect formation. Atomic structure in the vicinity of the defect has a greater deviation from a perfect SP^2 hybridized structure (planar with bond angles of 120° as in a graphene sheet) compared to perfect regions of a CNT. While stresses due to curvature are influenced by the radius of the CNT, stresses due to defect formation are affected by the type of defect.

It is observed in Fig. 6 that the stress concentration due to the presence of defects decreases at higher strains. In other words, with increased strain levels, the effect of defects in enhancing the local stress level decreases. Several investigators³⁵⁻³⁹ have observed the spontaneous formation of defects at higher strains. These studies have shown that the defected structures have a lower energy at higher strains.³⁸ A lowered energy is manifested by a lowered stress concentration effect.

Contrary to the stress concentration, the strain concentration at the defect increases as the applied strain is increased (see Fig. 7). In order to understand this, let us look more closely at the deformation pattern away from the defect and near the defect. Consider a defect free region as shown in Fig. 12(b). The basic hexagonal network is expected to stretch under the action of an axial load. As a result there is

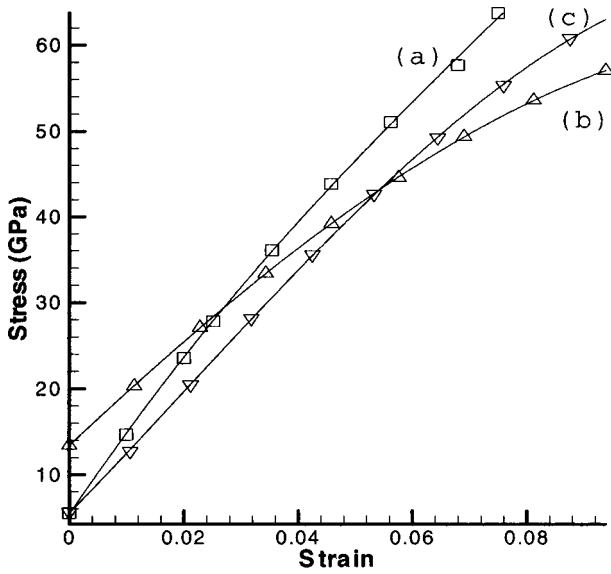


FIG. 9. Stress-strain curves for a (9,0) carbon tube with and without defects. (a) Stress-strain curve for a tube without defect. (b) Stress-strain curve for a type I defect. (c) Stress-strain curve for a type II defect.

a reduction in bond angles such as \widehat{UPQ} and a corresponding increase in bond angles such as \widehat{PQR} . The geometrical constraint due to the hexagonal nature of the mesh entails that an increase in angles \widehat{PQR} be about two times the decrease in angles \widehat{UPQ} as observed in Fig. 13. In addition, the bonds in the line of action of an axial load such as PY are expected to stretch, and bonds such as PQ stretch and rotate. The deformation induces predominantly longitudinal strains and compressive lateral strains due to Poisson's effect. Shear strains are caused by angle changes between any two perpendicular lines before and after deformation. Since the hexagon is extended in one direction and compressed in the other, this type of deformation does not induce any shear strain.

Now consider the region with a 5-7-7-5 defect as shown in Fig. 12(a). The defected regions comprise irregular heptagons and pentagons. Also the angles between bonds have considerable deviation from a perfect sp^2 structure (with a bond angle of 120°). It is intuitive to expect that a deformation of this high energy structure would occur by rearranging bond angles rather than bond lengths. Figure 14 shows bond angle changes for selected atoms near the defected region with respect to applied strains. A significant variation in bond

TABLE II. Stiffness of defected region of different nanotubes.

Nanotube	Radius (nm)	Chiral angle	Stiffness (TPa)
(9,0) (Defect Type I)	0.352	0°	0.621
(9,0) (Defect Type II)	0.352	0°	0.627
(10,0)	0.391	0°	0.639
(11,0)	0.431	0°	0.639
(13,0)	0.509	0°	0.638
(15,0)	0.587	0°	0.629
(5,5)	0.339	30°	0.524

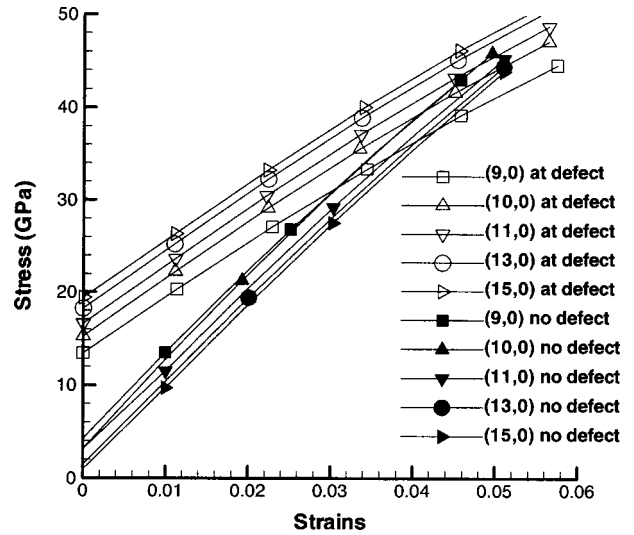


FIG. 10. Stress-strain curves for tubes of different diameters with and without defects. Stress-strain curves with filled symbols are for tubes without defects and stress-strain curves with open symbols are for tubes with defects.

angles is observed; for example there is an angular variation of up to 11% in \widehat{ABH} at an applied strain of 8% in contrast to a maximum angle variation of 4% in defect free structure for a (9,0) CNT. Larger changes in bond angles induce a larger component of rotation to the strain leading to higher longitudinal strains in the defected region. In addition, the irregularity of the heptagons and pentagons combined with large angular changes results in higher shear strain. As a result of these larger strains at lower stresses, the local stiffness of defected region is much lower than corresponding defect free regions. A fluctuation in the radius of curvature is observed at the defect. For example the radius of curvature at the defect varies from 3.45 to 3.53 Å in a (9,0) CNT with a radius of 3.523 Å. This fluctuation creates an instability at

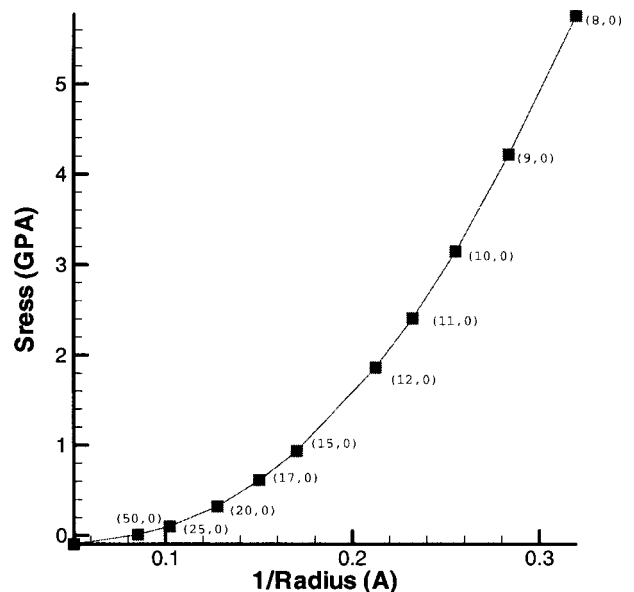


FIG. 11. Residual stress variation with radius.

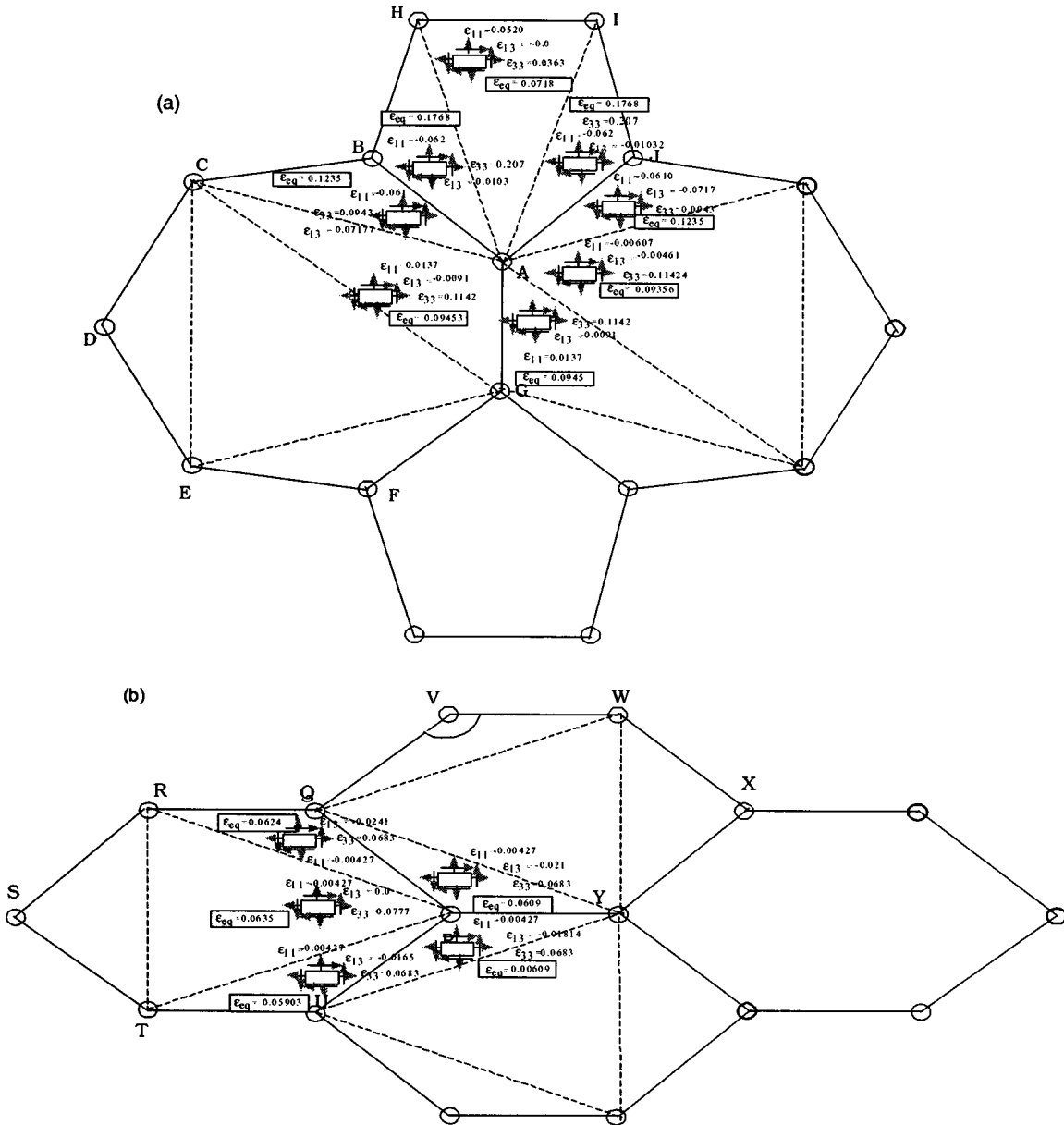


FIG. 12. (a) Atomic configuration of a 5-7-7-5 defect in a (9,0) carbon nanotube with a local variation of strains around one of the critical atoms. (b) Atomic configuration of a perfect region far away from the 5-7-7-5 defect in a (9,0) carbon nanotube with a local variation of strains around a typical atom. Dashed lines indicate subelement divisions.

the defect similar to a notch and contributes to the strain concentration and lowering of stiffness.

Stiffness reduction at the defect not only affects the elastic behavior, but is also expected to alter the inelastic behavior. The elastic behavior (for example, the Young's modulus) of a long nanotube with a few defects is marginally lowered because of the relatively low area fraction of the defects. However, plasticity, fracture, and failure are localized phenomena wherein the defects play a major role. It is now understood that the limiting behavior of nanotubes either for the onset of plasticity or for fracture is the generation of topological defects. Once the defects are nucleated they tend to serve as sites for further propagation of defects,³⁶ or result in crack propagation and brittle fracture¹⁸ depending on various factors such as the chirality and temperature.³⁸ Belytchko

*et al.*¹⁸ reported that there is a reduction in fracture stress in the presence of a 5-7-7-5 defect; in addition, the defect serves as a nucleation site for fracture. Defected regions of CNTs experience higher strains for similar values of stress compared to defect free tubes. The lower stiffness of the defect region studied here is a clear indication of a reduced load carrying capacity. This causes the higher localized strain concentrations responsible for failure at lower applied strains.

Local stiffness values of various CNTs with varying diameter are shown in Table II. It can be observed that there is very marginal difference in stiffness values for different $(n,0)$ types of nanotubes (0.621–0.639 TPa). However, the stiffness of the defect region in the (5,5) nanotube [comparable in diameter to the (9,0) CNT] is much lower (0.524

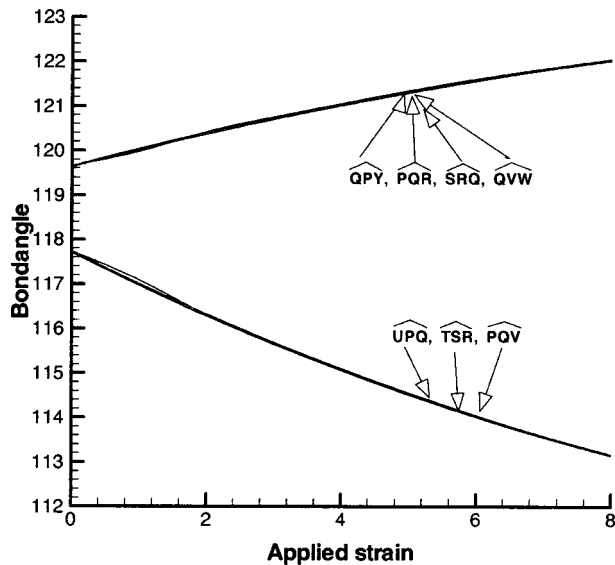


FIG. 13. Bond angle variation with applied strain for a few bond angles at a perfect region away from the defect.

TPa). This indicates that the curvature of the nanotube plays a minimal role in determining the mechanical behavior of the defected region. The lack of radial symmetry at the defect suggests an anisotropic behavior of the defect region. As a result the stiffness of the defect in the (5,5) tube is lower than the stiffness of other ($n,0$) types of tubes. It is interesting to note that the formation energy⁴⁰ of the defects is much higher for (5,5) nanotubes (3.34 eV) than ($n,0$) nanotubes (2.12–2.75 eV).

V. CONCLUSION

This paper demonstrates that atomic level stress and strain measures can be used to determine the Young's modulus of

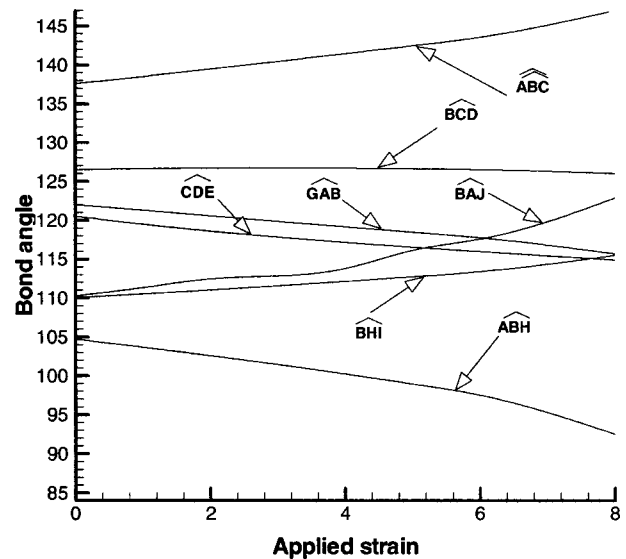


FIG. 14. Bond angle variation with applied strain for a few bond angles near a defected region.

carbon nanotubes. Further, these measures can be used effectively to evaluate the changes in mechanical behavior due to defects. The stiffness of defects reduces by about 30–50% and is dependent on a number of factors such as the chirality, the diameter, and the loading conditions.

ACKNOWLEDGMENTS

The authors wish to acknowledge the research collaborations with Professors Leon van Dommelen and Ashok Srinivasan during various phases of this work as a part of the Computational nanotechnology group at Florida State University. The funding provided by FSU Foundation is also gratefully acknowledged.

- ¹S. Iijima, *Nature (London)* **354**, 56 (1991).
- ²T. W. Ebbesen and T. Takada, *Carbon* **33**, 973 (1995).
- ³B. I. Yakobson, C. J. Brabec, and J. Bernholc, *Phys. Rev. Lett.* **76**, 2511 (1996).
- ⁴V. H. Crespi, M. L. Cohen, and A. Rubio, *Phys. Rev. Lett.* **79**, 2093 (1997).
- ⁵T. Kostyrko, M. Bartkowiak, and G. D. Mahan, *Phys. Rev. B* **59**, 3241 (1999).
- ⁶J. C. Charlier, T. W. Ebbesen, and P. Lambin, *Phys. Rev. B* **53**, 11 108 (1996).
- ⁷Z. Yao, H. W. C. Postma, L. Balents, C. Dekker, *Nature (London)* **402**, 6759 (1999).
- ⁸M. P. Allen and W. J. Tildesley, *Computer Simulation of Liquids* (Oxford University Press, Oxford, 1989).
- ⁹Z. S. Basinski, M. S. Duesberry, and R. Taylor, *Can. J. Phys.* **49**, 2160 (1971).
- ¹⁰J. F. Lutsko, *J. Appl. Phys.* **64**, 1152 (1988).
- ¹¹J. Cormier, J. M. Rickman, and T. J. Delph, *J. Appl. Phys.* **89**, 99 (2001).
- ¹²K. S. Cheung and S. Yip, *J. Appl. Phys.* **70**, 5688 (1996).
- ¹³D. Brenner, *Phys. Rev. B* **42**, 9458 (1990).
- ¹⁴W. Yu and A. Madhukar, *Phys. Rev. Lett.* **79**, 905 (1997).
- ¹⁵X. Y. Liu and J. B. Adams, *Acta Mater.* **46**, 3467 (1998).
- ¹⁶S. Namilaie, N. Chandra, and T. G. Nieh, *Scanning Microsc.* **46**, 49 (2001).
- ¹⁷T. Halicioglu, *Thin Solid Films* **312**, 11 (1998).
- ¹⁸T. Belytschko, S. P. Xiao, G. C. Schatz, and R. S. Ruoff, *Phys. Rev. B* **65**, 235430 (2002).
- ¹⁹Y. Xia, M. Zhao, Y. Ma, M. Ying, X. Liu, P. Liu, and L. Mei, *Phys. Rev. B* **65**, 155415 (2002).
- ²⁰B. A. Galanov, S. B. Galanov, and Y. Gogotsi, *J. Nanoparticle Res.*, **4**, 207 (2002).
- ²¹O. C. Zienkiewicz, *The Finite Element Method* (TMH, New Delhi, 1979).
- ²²E. Hernandez, C. Goze, P. Bernier, and A. Rubio, *Appl. Phys. A: Solids Surf.* **68**, 287 (1999).
- ²³D. Qian, W. K. Liu, and R. S. Ruoff, *J. Phys. Chem. B* **105**, 10 753 (2001).

- ²⁴G. Zhou, W. Duan, and B. Gu, *Chem. Phys. Lett.* **333**, 344 (2001).
- ²⁵A. Krishnan, E. Dujardin, T. W. Ebbesen, P. N. Yianilos, and M. M. J. Treacy, *Phys. Rev. B* **58**, 14 013 (2001).
- ²⁶J. P. Lu, *Phys. Rev. Lett.* **79**, 1297 (1997).
- ²⁷B. G. Demczyk, Y. M. Wang, J. Cumings, M. Hetman, W. Han, A. Zettl, and R. O. Ritchie, *Mater. Sci. Eng., A* **334**, 173 (2002).
- ²⁸G. V. Lier, C. V. Alsenoy, V. V. Doren, and P. Gerrlings, *Chem. Phys. Lett.* **326**, 181 (2000).
- ²⁹Z. C. Tu and Z. C. O. Yang, *Phys. Rev. B* **65**, 233407 (2002).
- ³⁰M. M. J. Treacy, T. W. Ebbesen, and J. M. Gibbson, *Nature (London)* **381**, 678 (1996).
- ³¹J. P. Salvetat, G. A. D. Briggs, J. M. Bonard, R. R. Bacsa, A. J. Kulik, T. Stockli, Nancy A. Burnham, and L. Forro, *Phys. Rev. Lett.* **82**, 944 (1999).
- ³²N. Yao and V. Lordi, *J. Appl. Phys.* **84**, 1939 (1998).
- ³³C. F. Cornwell and L. T. Wille, *Solid State Commun.* **101**, 555 (1997).
- ³⁴D. H. Robertson, D. W. Brenner, and J. W. Mintmire, *Phys. Rev. B* **45**, 12 592 (1992).
- ³⁵B. I. Yakobson, C. J. Brabec, and J. Bernholc, *Phys. Rev. B* **76**, 2511 (1996).
- ³⁶M. B. Nardelli, B. I. Yakobson, and J. Bernholc, *Phys. Rev. B* **57**, R4277 (1998).
- ³⁷C. Wei, K. Cho, and D. Srivastava, *Phys. Rev. B* **67**, 115407 (2003).
- ³⁸M. B. Nardelli, B. I. Yakobson, and J. Bernholc, *Phys. Rev. Lett.* **81**, 4656 (1998).
- ³⁹P. Zhang, P. E. Lammert, and V. H. Crespi, *Phys. Rev. Lett.* **81**, 5346 (1998).
- ⁴⁰B. C. Pan, W. S. Yang, and J. Yang, *Phys. Rev. B* **62**, 12 652 (2000).